0026-895X/03/6305-1032–1042$7.00
MOLECULAR PHARMACOLOGY
Copyright © 2003 The American Society for Pharmacology and Experimental Therapeutics
Mol Pharmacol 63:1032–1042, 2003

Vol. 63, No. 5
2054/1060488
Printed in U.S.A.

Fatty Alcohol Phosphates are Subtype-Selective Agonists and Antagonists of Lysophosphatidic Acid Receptors

TAMAS VIRAG, DON B. ELROD,[1] KAROLY LILIOM, VINEET M. SARDAR, ABBY L. PARRILL, KAZUAKI YOKOYAMA, GANGADHAR DURGAM, WENLIN DENG, DUANE D. MILLER, and GABOR TIGYI

Departments of Physiology (T.V., K.Y., W.D. G.T.) and Pharmaceutical Sciences (D.B.E., G.D., D.D.M.), University of Tennessee Health Science Center, Memphis, Tennessee; Department of Chemistry and Computational Research on Materials Institute, University of Memphis, Memphis, Tennessee (V.M.S., A.L.P.); and Institute of Enzymology, Hungarian Academy of Sciences, Budapest, Hungary (K.L.)

Received August 5, 2002; accepted February 7, 2003

This article is available online at http://molpharm.aspetjournals.org

ABSTRACT

A more complete understanding of the physiological and pathological role of lysophosphatidic acid (LPA) requires receptor subtype-specific agonists and antagonists. Here, we report the synthesis and pharmacological characterization of fatty alcohol phosphates (FAP) containing saturated hydrocarbon chains from 4 to 22 carbons in length. Selection of FAP as the lead structure was based on computational modeling as a minimal structure that satisfies the two-point pharmacophore developed earlier for the interaction of LPA with its receptors. Decyl and dodecyl FAPs (FAP-10 and FAP-12) were specific agonists of LPA_2 (EC_{50} = 3.7 ± 0.2 μM and 700 ± 22 nM, respectively), yet selective antagonists of LPA_3 (K_i = 90 nM for FAP-12) and FAP-12 was a weak antagonist of LPA_1. Neither LPA_1 nor LPA_3 receptors were activated by FAPs; in contrast, LPA_2 was activated by FAPs with carbon chains between 10 and 14. Computational modeling was used to evaluate the interaction between individual FAPs (8 to 18) with LPA_2 by docking each compound in the LPA binding site. FAP-12 displayed the lowest docked energy, consistent with its lower observed EC_{50}. The inhibitory effect of FAP showed a strong hydrocarbon chain length dependence with C12 being optimum in the *Xenopus laevis* oocytes and in LPA_3-expressing RH7777 cells. FAP-12 did not activate or interfere with several other G-protein-coupled receptors, including S1P-induced responses through $S1P_{1,2,3,5}$ receptors. These data suggest that FAPs are ligands of LPA receptors and that FAP-10 and FAP-12 are the first receptor subtype-specific agonists for LPA_2.

Lysophosphatidic acid (LPA) is a member of the phospholipid growth factor (PLGF) family. PLGFs exert pleiotropic biological effects, such as activating platelet aggregation and affecting cell proliferation, apoptosis, migration, and cell shape (for reviews, see Goetzl et al., 2000; Tigyi, 2001). LPA elicits its biological effects through the activation of G protein-coupled receptors. In mammalian cells, three LPA-specific receptors have been identified, including LPA_1 (EDG-2), LPA_2 (EDG-4) and LPA_3 (EDG-7), all members of the endothelial differentiation gene (EDG) family (for review, see Contos et al., 2000). In addition to LPA_1, the PSP24 receptor was shown to elicit LPA-induced Ca^{2+}-dependent Cl^--currents in *Xenopus laevis* oocytes (Guo et al., 1996; Fischer et al., 1998; Kimura et al., 2001). Receptors LPA_{1-3} share 50 to 54% sequence identity (Chun et al., 2002). The EDG receptor family also contains five other receptors, $S1P_{1-5}$ (EDG-1, -5, -3, -6, -8), specific for the sphingolipid PLGF sphingosine 1-phosphate (S1P) (Chun et al., 2002). The S1P receptors $S1P_{1-5}$ share 50% amino acid sequence identity and 35% identity with the LPA receptors (Chun et al., 2002), suggesting possible similarities in the characteristics of ligand recognition in these receptors. Most cells express a combination of these receptors, making it difficult to dissect the biological effects mediated by an individual receptor subtype. The need to understand the biological function of PLGF receptors and the desire to pharmacologically exploit the differences in their ligand recognition requires the development of receptor subtype-specific agonists and antagonists. Until recently, no such compounds were available. Local and general anesthetics have been reported to inhibit PLGF receptors in *X. laevis* oocytes (Chan and Durieux, 1997; Tigyi et al., 1997). Likewise, *N*-acyl serine phosphoric acid and *N*-acyl tyrosine phosphoric acid were shown to inhibit LPA-induced platelet aggregation, Cl^--currents in *X. laevis* oocytes, and neutrophil adhesion to vascular endothelial cells (Sugiura et al., 1994; Liliom et al., 1996a; Hooks et al., 1998; Siess et al., 1999). However, in MDA MB231 cells, *N*-acyl serine phosphoric acid

This work was supported in part by grants HL61469 and CA92160 from the National Institutes of Health.

[1] Current address: Lynntech, Inc., College Station, TX 77840.

ABBREVIATIONS: LPA, lysophosphatidic acid; EDG, endothelial differentiation gene; FAP, fatty alcohol phosphate; GPCR, G protein-coupled receptor; GTP-γ-S, guanosine 5′-3-*O*-(thio)triphosphate; MS, mass spectrometry; LPP, lipid phosphate phosphatase; PLGF, phospholipid growth factor; S1P, sphingosine 1-phosphate; RT-PCR, reverse transcription-polymerase chain reaction.

was shown to be a potent activator of LPA-like responses (Hooks et al., 1998), although the receptor activated by this compound was not identified. This same compound was a weak agonist of LPA_1 and LPA_3 receptors heterologously expressed in Jurkat T cells (An et al., 1998). Cyclic phosphatidic acid was also shown to inhibit LPA-induced platelet aggregation (Gueguen et al., 1999); however, it is an LPA receptor agonist in *X. laevis* oocytes (Liliom et al., 1996b; Fischer et al., 1998) and in cells that heterologously express EDG family LPA receptors (Bandoh et al., 2000).

Computational models for $S1P_1$ (Parrill et al., 2000), LPA_1, and LPA_2 (Wang et al., 2001; Sardar et al., 2002) confirmed the importance of two specific interactions between each receptor and its phospholipid ligand. One of these interactions involves ion pairing between the phosphate group of LPA and two positively charged conserved residues in the third and seventh putative transmembrane segments of the LPA receptor subfamily. A second interaction involves hydrophobic residues within the transmembrane segment of the receptor and the hydrophobic tail of LPA (Fischer et al., 2001). Based on these two points of interaction with the LPA pharmacophore, we identified dioctylglycerol pyrophosphate and dioctyl-phosphatidic acid as selective antagonists of LPA_1 and LPA_3 receptors, with an order of magnitude higher potency for LPA_3 (Fischer et al., 2001). A stereoisomer of the 2-substituted *N*-acyl ethanolamide phosphate LPA analog containing a bulky benzyl-4-oxybenzyl group was shown to be a dual LPA_1/LPA_3 competitive antagonist with higher inhibitory potency for LPA_1 (Heise et al., 2001).

Herein we report the synthesis and characterization of fatty alcohol phosphates (FAPs) that lack a glycerol backbone and therefore consist of only a polar phosphate head group and a hydrophobic tail and represent a minimal structure that satisfies the two-point pharmacophore introduced earlier for LPA-like structures (Fischer et al., 2001, Sardar et al., 2002). Pharmacological characterization of the ligand properties of FAPs showed an exquisite dependence on the length of the hydrocarbon chain. FAPs with 10, 12, and 14 carbons are agonists for LPA_2 and antagonists for the LPA_3 receptor. In contrast, other FAPs, with carbon chain lengths of 4, 8, 16, 18, and 22, showed no agonist effect on any mammalian LPA receptor. FAP-14 and FAP-18 were weak antagonists of the LPA_3 receptor, along with FAP-10.

Materials and Methods

Materials

Lipids were purchased from Avanti Polar Lipids (Alabaster, AL); other chemicals and fetal bovine serum were obtained from Sigma-Aldrich Chemical Co. (St. Louis, MO). Cell culture medium (Dulbecco's modified Eagle's medium) and G418 were purchased from Cellgro (Herndon, VA). Fura-2 acetoxymethyl ester was from Molecular Probes (Eugene, OR). Oocyte positive *X. laevis* frogs were from Xenopus I (Dexter, MI). Collagenase A was purchased from Roche Molecular Biochemicals (Mannheim, Germany). [^{35}S]GTP-γ-S was purchased from Amersham Biosciences (Uppsala, Sweden). FLAG epitope-tagged cDNAs encoding human LPA_2 and LPA_3 receptors in pCDNA3 plasmids (Invitrogen, Carlsbad, CA) were a gift from Dr. Junken Aoki (University of Tokyo, Tokyo, Japan). $S1P_1$ cDNA was a gift from Dr. Timothy Hla (University of Connecticut, Storres, CT). PCDNA3.1 expression vector containing $S1P_5$ cDNA was a gift from Dr. Kevin Lynch (University of Virginia, Charlottesville, VA).

Chemical Synthesis of the FAP Compounds

All reagents and chromatography media were purchased from Sigma-Aldrich Chemical Co. or Fisher Scientific (Pittsburgh, PA) and were used without further purification. Thin-layer chromatography was performed on 200-μm alumina plates (Silica gel 60 Å; E.M. Science, Hawthorne, NY). Flash chromatography was performed on silica gel (60 Å, 200–425 mesh). Melting points were determined on a Thomas-Hoover capillary melting point apparatus and are uncorrected. ^{1}H, ^{13}C, and ^{31}P nuclear magnetic resonance spectra were obtained on an AX 300 spectrometer (Bruker, Billerica, MA). Chemical shifts for ^{1}H and ^{13}C are reported as parts per million relative to tetramethylsilane. Spectra for ^{31}P are reported as parts per million relative to 0.0485 M triphenylphosphate in $CDCl_3$. Electrospray ionization liquid chromatography/mass spectrometry was performed on a Bruker Esquire LC/MS system.

Synthesis of Phosphoric Acid Dibenzyl Ester Alkyl Esters (1–8a)

The synthesis of protected alkyl monophosphates (Fig. 1) was performed according to the method of Bittman et al. (1996) except that peracetic acid was used for the oxidation step instead of *m*-chloroperoxybenzoic acid. Each anhydrous alcohol (1.0 mmol) and 365 mg (5.17 mmol) of 1*H*-tetrazole were dissolved in 34 ml of anhydrous methylene chloride. A solution of 0.895 g (2.58 mmol) of dibenzyl-*N*,*N*-diisopropyl phosphoramidite in 5 ml of anhydrous methylene chloride was added under an argon atmosphere. The reaction mixture was stirred at room temperature for 2 h and was then cooled to −38°C in an isopropyl alcohol/dry ice bath. Peracetic acid [0.815 g (3.43 mmol) of 32% acid] in 28 ml of anhydrous methylene chloride was added drop-wise, and the temperature of the reaction mixture was raised to 0°C and stirred for 1 h. To the reaction mixture, 200 ml of methylene chloride was added, and the organic layer was washed with 10% sodium metabisulfite (2 × 40 ml), saturated sodium bicarbonate (2 × 40 ml), water (30 ml), and brine (40 ml). The organic layer was dried with anhydrous sodium sulfate, filtered, and concentrated under vacuum to dryness. The resulting crude products were purified by silica gel chromatography using hexane/ethyl acetate (1:1 for 1a and 7:3 for 2–8a) to elute the desired product.

Spectral Characterization of Phosphoric Acid Dibenzyl Ester Alkyl Esters (1–8a)

1a Isolated As a Clear Oil (309 mg) That Was Contaminated with Excess Phosphorylating Reagent). ^{1}H NMR ($CDCl_3$) δ 0.88 (t, J = 7.2 Hz, 3H, $C\underline{H}_3$), 1.34 (sextet, J = 7.2 Hz, 2H, $OCH_2CH_2C\underline{H}_2CH_3$), 1.59 (quintet, J = 6.6 Hz, 2H, $OCH_2C\underline{H}_2CH_2CH_3$), 3.99 (q, 6.6 Hz, 2H, $OC\underline{H}_2CH_2CH_2CH_3$), 5.02 (d, J = 1.8 Hz, 2H, $OC\underline{H}_2Ar$), 5.05 (d, J = 2.1 Hz, 2H, $OC\underline{H}_2Ar$), 7.35 (br s, 10H, 2 × Ar$\underline{H}$); ^{13}C NMR ($CDCl_3$) δ 13.55, 18.60, 32.16 (d, $J_{C,P}$ = 6.8 Hz), 67.72 (d, $J_{C,P}$ = 6.1 Hz), 69.13(d, $J_{C,P}$ = 5.5 Hz), 127.90, 128.47, 128.55, 136.00 (d, $J_{C,P}$ = 6.8 Hz); ^{31}P NMR ($CDCl_3$) δ 16.84; MS: [M + ^{23}Na] at *m*/*z* 357.3.

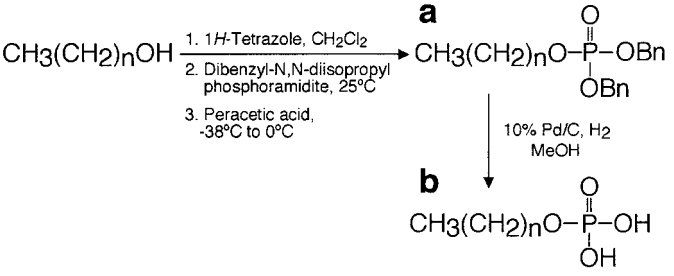

Fig. 1. The synthesis of FAPs. 1, FAP-4, n = 3; 2, FAP-8, n = 7; 3, FAP-10, n = 9; 4, FAP-12, n = 11; 5, FAP-14, n = 13; 6, FAP-16, n = 15; 7, FAP-18, n = 17; 8, FAP-22, n = 21.

2a Isolated As a Clear Oil (351 mg, 90% Yield). ^{1}H NMR ($CDCl_3$) δ 0.88 (t, J = 6.9 Hz, 3H,$C\underline{H}_3$), 1.24 (br s, 10H, $OCH_2CH_2(C\underline{H}_2)_5CH_3$), 1.60 (quintet, J = 6.9 Hz, 2H, $OCH_2C\underline{H}_2(CH_2)_5CH_3$), 3.98 (q, J = 6.6 Hz, 6.9 Hz, 2H, $OC\underline{H}_2CH_2(CH_2)_5CH_3$), 5.02 (d, J = 2.1 Hz, 2H, $OC\underline{H}_2Ar$), 5.05 (d, J = 2.4 Hz, 2H $OC\underline{H}_2Ar$), 7.34 (br s, 10H, 2 × Ar$\underline{H}$); ^{13}C NMR ($CDCl_3$) δ 14.09, 22.62, 25.38, 29.06, 29.14, 30.17 (d, $J_{C,P}$ = 6.9 Hz), 31.75, 68.05 (d, $J_{C,P}$ = 6.2 Hz), 69.12 (d, $J_{C,P}$ = 5.5 Hz), 127.90, 128.47, 128.56, 135.97 (d, $J_{C,P}$ = 6.9 Hz); ^{31}P NMR ($CDCl_3$) δ 16.83; MS: $[M + {}^{23}Na]^+$ at *m/z* 413.4.

3a Isolated As a Clear Oil (334 mg, 80% Yield). ^{1}H NMR ($CDCl_3$) δ 0.88 (t, J = 6.9 Hz, 3H,$C\underline{H}_3$), 1.24 (br s, 14H, $OCH_2CH_2(C\underline{H}_2)_7CH_3$), 1.58 (quintet, J = 6.9 Hz, 2H, $OCH_2C\underline{H}_2(CH_2)_7CH_3$), 3.98 (q, J = 6.7 Hz, 2H, $OC\underline{H}_2CH_2(CH_2)_7CH_3$), 5.02 (d, J = 2.2 Hz, 2H, $OC\underline{H}_2Ar$), 5.04 (d, J = 2.3 Hz, 2H $OC\underline{H}_2Ar$), 7.34 (br s, 10H, 2 × Ar$\underline{H}$); ^{13}C NMR ($CDCl_3$) δ 13.56, 22.13, 24.85, 28.57, 28.75, 28.95 (d, $J_{C,P}$ = 1.6 Hz), 29.65 (d, $J_{C,P}$ = 6.9 Hz), 31.34, 67.52 (d, $J_{C,P}$ = 6.1 Hz), 68.59 (d, $J_{C,P}$ = 5.6 Hz), 126.40, 126.97, 127.35, 127.96 (d, $J_{C,P}$ = 6.6 Hz), 135.47 (d, $J_{C,P}$ = 6.8 Hz); ^{31}P NMR ($CDCl_3$) δ 16.82; MS: $[M + {}^{23}Na]^+$ at *m/z* 441.4.

4a Isolated As a Clear Oil (361 mg, 81% Yield). ^{1}H NMR ($CDCl_3$) δ 0.88 (t, J = 7.2 Hz, 3H, $C\underline{H}_3$), 1.24 (br s, 18 H, $OCH_2CH_2(C\underline{H}_2)_9CH_3$), 1.60 (quintet, J = 6.9 Hz, 2H, $OCH_2C\underline{H}_2(CH_2)_9CH_3$), 3.98 (q, J = 6.9 Hz, 2H, $OC\underline{H}_2CH_2(CH_2)_9CH_3$), 5.02 (d, J = 2.1 Hz, 2H, $OC\underline{H}_2Ar$), 5.05 (d, J = 2.1 Hz, 2H, $OC\underline{H}_2Ar$), 7.34 (br s, 10H, 2 × Ar$\underline{H}$); ^{13}C NMR ($CDCl_3$) δ 14.13, 22.69, 25.38, 29.12, 29.35, 29.49, 29.56, 29.63, 30.18 (d, $J_{C,P}$ = 7.0 Hz), 31.92, 68.05 (d, $J_{C,P}$ = 6.1 Hz), 69.12 (d, $J_{C,P}$ = 5.4 Hz), 127.89, 128.46, 128.55, 135.97 (d, $J_{C,P}$ = 6.8 Hz); ^{31}P NMR ($CDCl_3$) δ 16.84; MS: $[M + {}^{23}Na]^+$ at *m/z* 469.1.

5a Isolated As a Clear Oil (384 mg, 81% Yield). ^{1}H NMR ($CDCl_3$) δ 0.88 (t, J = 6.9 Hz, 3H, $C\underline{H}_3$), 1.27 (br s, 22 H, $OCH_2CH_2(C\underline{H}_2)_{11}CH_3$), 1.64 (quintet, J = 6.8 Hz, 2H, $OCH_2C\underline{H}_2(CH_2)_{11}CH_3$), 3.98 (q, J = 6.9 Hz, 2H, $OC\underline{H}_2CH_2(CH_2)_{11}CH_3$), 5.04 (d, J = 2.1 Hz, 2H, $OC\underline{H}_2Ar$), 5.06 (d, J = 2.1 Hz, 2H, $OC\underline{H}_2Ar$), 7.34 (br s, 10H, 2 × Ar$\underline{H}$); ^{13}C NMR ($CDCl_3$) δ 13.55, 22.14, 24.85, 25.26, 28.57, 28.80, 28.98 (d, $J_{C,P}$ = 5.2 Hz), 29.12 (m), 29.65 (d, $J_{C,P}$ = 6.9 Hz), 31.38, 32.31, 62.41, 67.50 (d, $J_{C,P}$ = 6.1 Hz), 68.59 (d, $J_{C,P}$ = 5.6 Hz), 127.34, 127.95 (d, $J_{C,P}$ = 6.8 Hz), 135.48 (d, $J_{C,P}$ = 6.8 Hz); ^{31}P NMR ($CDCl_3$) δ 16.85; MS: $[M + {}^{23}Na]^+$ at *m/z* 497.2.

6a Isolated As a Clear Oil (427 mg, 85% Yield). ^{1}H NMR ($CDCl_3$) δ 0.88 (t, J = 6.9 Hz, 3H, $C\underline{H}_3$), 1.28 (br s, 26H, $OCH_2CH_2(C\underline{H}_2)_{13}CH_3$), 1.62 (quintet, J = 6.9 Hz, 2H, $OCH_2C\underline{H}_2(CH_2)_{13}CH_3$), 3.99 (q, J = 6.9 Hz, 2H, $OC\underline{H}_2CH_2(CH_2)_{13}CH_3$), 5.04 (d, J = 2.1 Hz, 2H, $OC\underline{H}_2Ar$), 5.07 (d, J = 2.1 Hz, 2H, $OC\underline{H}_2Ar$), 7.35 (br s, 10H, 2 × Ar$\underline{H}$); ^{13}C NMR ($CDCl_3$) δ 13.57, 22.15, 24.85, 28.58, 28.83, 28.99 (d, $J_{C,P}$ = 6.8 Hz), 29.17, 29.66 (d, $J_{C,P}$ = 6.9 Hz), 31.39, 67.49 (d, $J_{C,P}$ = 6.1 Hz), 68.59 (d, $J_{C,P}$ = 5.6 Hz), 127.35, 127.95 (d, $J_{C,P}$ = 6.6 Hz), 135.48 (d, $J_{C,P}$ = 6.8 Hz); ^{31}P NMR ($CDCl_3$) δ 16.88; MS: $[M + {}^{23}Na]^+$at *m/z* 525.3.

7a Isolated As a Hygroscopic White Solid (474 mg, 89% Yield), mp 32–33°C. ^{1}H NMR ($CDCl_3$) δ 0.88 (t, J = 6.9 Hz, 3H, $C\underline{H}_3$), 1.25 (br s, 30H, $OCH_2CH_2(C\underline{H}_2)_{15}CH_3$), 1.60 (quintet, J = 6.9 Hz, 2H, $OCH_2C\underline{H}_2(CH_2)_{15}CH_3$), 3.98 (q, J = 6.9 Hz, 2H, $OC\underline{H}_2CH_2(CH_2)_{15}CH_3$), 5.02 (d, J = 2.1 Hz, 2H, $OC\underline{H}_2Ar$), 5.05 (d, J = 2.1 Hz, 2H, $OC\underline{H}_2Ar$), 7.34 (br s, 10H, 2 × Ar$\underline{H}$); ^{13}C NMR ($CDCl_3$) δ 14.12, 22.70, 25.40, 29.13, 29.38, 29.51, 29.58, 29.68, 29.72, 30.20 (d, $J_{C,P}$ = 6.9 Hz), 31.94, 68.06 (d, $J_{C,P}$ = 6.1 Hz), 69.14 (d, $J_{C,P}$ = 5.4 Hz), 127.90, 128.47, 128.55, 136.00 (d, $J_{C,P}$ = 6.8 Hz).; ^{31}P NMR ($CDCl_3$) δ 16.83; MS: $[M + {}^{23}Na]^+$at *m/z* 553.3.

8a Isolated As a Hygroscopic White Solid (516 mg, 88% Yield), mp 43.5–44.5°C. ^{1}H NMR ($CDCl_3$) δ 0.88 (t, J = 6.9 Hz, 3H, $C\underline{H}_3$), 1.25 (br s, 38H, $OCH_2CH_2(C\underline{H}_2)_{19}CH_3$), 1.60 (quintet, J = 6.9 Hz, 2H, $OCH_2C\underline{H}_2(CH_2)_{19}CH_3$), 3.98 (q, J = 6.6 Hz, 2H, $OC\underline{H}_2CH_2(CH_2)_{19}CH_3$), 5.02 (d, J = 2.4 Hz, 2H, $OC\underline{H}_2Ar$), 5.05 (d, J = 2.4 Hz, 2H, , $OC\underline{H}_2Ar$), 7.35 (br s, 10H, 2 × ArH); ^{13}C NMR ($CDCl_3$) δ 14.13, 22.70, 25.39, 29.12, 29.37, 29.50, 29.57, 29.66, 29.71, 30.18(d, $J_{C,P}$ = 6.9 Hz), 31.93, 68.06 (d, $J_{C,P}$ = 6.0 Hz), 69.13 (d, $J_{C,P}$ = 5.6 Hz), 127.89, 128.47, 128.55, 135.98 (d, $J_{C,P}$ = 6.9 Hz); ^{31}P NMR ($CDCl_3$) δ 16.83; MS: $[M + {}^{23}Na]^+$ at *m/z* 609.3.

Synthesis of Phosphoric Acid Mono Alkyl Esters (1–8b)

200 mg of 1–8a was dissolved in 30 ml of anhydrous methanol in a pressure vessel (Fig. 1). The vessel was purged with argon and ~200 mg of 10% Pd/C catalyst was added. The vessel was connected to a hydrogenation apparatus and a hydrogen atmosphere of ~ 50 psi was maintained inside the reaction vessel at room temperature for 8 h. The reaction mixture was then filtered by vacuum through a pad of methanol-washed celite. Solvent was evaporated under vacuum, yielding the desired product.

Spectral Characterization of Phosphoric Acid Mono alkyl Esters (1–8b)

1b Isolated As a Yellow Oil (70 mg, 86% Yield). ^{1}H NMR ($CDCl_3$/MeOH-d_4) δ 0.95 (t, J = 7.2 Hz, 3H, $C\underline{H}_3$), 1.43 (sextet, J = 7.5 Hz, 2H, $OCH_2CH_2C\underline{H}_2CH_3$), 1.66 (quintet, J = 6.9, 2H, $OCH_2C\underline{H}_2CH_2CH_3$), 3.99 (q, J = 6.6 Hz, 2H, $OC\underline{H}_2CH_2CH_2CH_3$); ^{13}C NMR ($CDCl_3$/MeOH-$d_4$) δ 13.71, 19.02, 32.72 (d, $J_{C,P}$ = 7.2 Hz), 66.86 (d, $J_{C,P}$ = 5.5 Hz); ^{31}P NMR ($CDCl_3$/MeOH-d_4) δ 18.84; MS: $[M - H]^-$ at *m/z* 153.0.

2b Isolated As a White/Yellow Tacky Solid (100 mg, 93% Yield). ^{1}H NMR ($CDCl_3$/MeOH-d_4) δ 0.89 (t, J = 6.9 Hz, 3H, $C\underline{H}_3$), 1.29 (br s, 10H, $OCH_2CH_2(C\underline{H}_2)_5CH_3$), 1.67 (quintet, J = 6.9 Hz, 2H, $OCH_2C\underline{H}_2(CH_2)_5CH_3$), 3.97 (q, J = 6.6 Hz, 2H, $OC\underline{H}_2CH_2(CH_2)_5CH_3$); ^{13}C NMR ($CDCl_3$/MeOH-$d_4$) δ 14.18, 22.98, 25.89, 29.57, 29.58, 30.76 (d, $J_{C,P}$ = 7.3 Hz), 32.18, 67.16 (d, $J_{C,P}$ = 5.2 Hz); ^{31}P NMR ($CDCl_3$/MeOH-d_4) δ 20.55; MS: $[M - H]^-$ at *m/z* 209.1.

3b Isolated As a White/Yellow Tacky Solid (102 mg, 90% Yield). ^{1}H NMR ($CDCl_3$/MeOH-d_4) δ 0.89 (t, J = 6.9 Hz, 3H, $C\underline{H}_3$), 1.28 (br s, 14 H, $OCH_2CH_2(C\underline{H}_2)_7CH_3$), 1.67 (quintet, J = 6.8 Hz, 2H, $OCH_2C\underline{H}_2(CH_2)_7CH_3$), 3.97 (q, J = 6.9 Hz, 2H, $OC\underline{H}_2CH_2(CH_2)_7CH_3$); ^{13}C NMR ($CDCl_3$/MeOH-$d_4$) δ 12.83, 21.86, 24.79, 28.51 (d, $J_{C,P}$ = 5.9 Hz), 28.79 (d, $J_{C,P}$ = 1.3 Hz), 29.66 (d, $J_{C,P}$ = 7.2 Hz), 31.12, 65.97 (d, $J_{C,P}$ = 5.6 Hz); ^{31}P NMR (DMSO-d_6) δ 16.55; MS: $[M - H]^-$ at *m/z* 236.9.

4b Isolated As a White Solid (112 mg, 94% Yield). ^{1}H NMR ($CDCl_3$/MeOH-d_4) δ 0.88 (t, J = 6.6 Hz, 3H, $C\underline{H}_3$), 1.27 (br s, 18 H, $OCH_2CH_2(C\underline{H}_2)_9CH_3$), 1.67 (quintet, J = 6.6 Hz, 2H, $OCH_2C\underline{H}_2(CH_2)_9CH_3$), 3.97 (q, J = 6.6 Hz, 2H, $OC\underline{H}_2CH_2(CH_2)_9CH_3$); ^{13}C NMR ($CDCl_3$/MeOH-$d_4$) δ 14.21, 22.98, 25.84, 29.57, 29.67, 29.89, 29.92, 29.96, 29.98, 30.69 (d, $J_{C,P}$ = 7.4 Hz), 32.25, 67.22 (d, $J_{C,P}$ = 5.7 Hz); ^{31}P NMR ($CDCl_3$/MeOH-d_4) δ 21.22; MS: $[M - H]^-$ at *m/z* 265.0.

5b Isolated As a White Solid (105 mg, 85% Yield), mp 58–60°C. ^{1}H NMR ($CDCl_3$/MeOH-d_4) δ 0.89 (t, J = 6.9 Hz, 3H, $C\underline{H}_3$), 1.27 (br s, 22 H, $OCH_2CH_2(C\underline{H}_2)_{11}CH_3$), 1.64 (quintet, J = 6.8 Hz, 2H, $OCH_2C\underline{H}_2(CH_2)_{11}CH_3$), 3.96 (q, J = 6.9 Hz, 2H, $OC\underline{H}_2CH_2(CH_2)_{11}CH_3$); ^{13}C NMR ($CDCl_3$/MeOH-$d_4$) δ 12.66, 21.82, 24.75, 28.48 (d, $J_{C,P}$ = 8.5 Hz), 28.78 (d, $J_{C,P}$ = 1.3 Hz), 28.85, 29.62 (d, $J_{C,P}$ = 7.2 Hz), 31.14, 65.88 (d, $J_{C,P}$ = 5.7 Hz); ^{31}P NMR (DMSO-d_6) δ 16.51; MS: $[M - H]^-$ at *m/z* 293.0.

6b Isolated As a White Solid (118 mg, 92% Yield), mp 71–72°C. ^{1}H NMR ($CDCl_3$/MeOH-d_4) δ 0.89 (t, J = 6.9 Hz, 3H, $C\underline{H}_3$), 1.28 (br s, 26 H, $OCH_2CH_2(C\underline{H}_2)_{13}CH_3$), 1.64 (quintet, J = 6.8 Hz, 2H, $OCH_2C\underline{H}_2(CH_2)_{13}CH_3$), 3.96 (q, J = 6.9 Hz, 2H, $OC\underline{H}_2CH_2(CH_2)_{13}CH_3$); ^{13}C NMR ($CDCl_3$/MeOH-$d_4$) δ 12.77, 21.85, 24.77, 28.48 (d, $J_{C,P}$ = 8.5 Hz), 28.80 (d, $J_{C,P}$ = 1.3 Hz), 28.88, 29.64 (d, $J_{C,P}$ = 7.3 Hz), 31.16, 65.94 (d, $J_{C,P}$ = 5.7 Hz); ^{31}P NMR (DMSO-d_6) δ 16.51; MS: $[M - H]^-$ at *m/z* 321.0.

7b Isolated As a White Solid (104 mg, 79% Yield). ^{1}H NMR ($CDCl_3$/MeOH-d_4) δ 0.89 (t, J = 6.9 Hz, 3H, $C\underline{H}_3$), 1.27 (br s, 30H, $OCH_2CH_2(C\underline{H}_2)_{15}CH_3$), 1.68 (quintet, J = 6.9 Hz, 2H, $OCH_2C\underline{H}_2(CH_2)_{15}CH_3$); 3.98 (q, J = 6.9 Hz, 2H,

$OCH_2CH_2(CH_2)_{15}CH_3$); ^{13}C NMR ($CDCl_3$/MeOH-d_4) δ 14.26, 23.14, 26.01, 29.74, 29.84, 30.06, 30.09, 30.16, 30.87 (d, $J_{C,P}$ = 7.2 Hz), 32.42, 67.32 (d, $J_{C,P}$ = 5.8 Hz); ^{31}P NMR ($CDCl_3$/MeOH-d_4) δ 21.69; MS: $[M - H]^-$ at m/z 349.1.

8b Isolated As a White Solid (98 mg, 71% Yield). ^1H NMR ($CDCl_3$/MeOH-d_4) δ 0.88(t, J = 6.9 Hz, 3H), 1.26 (br s, 38H, $OCH_2CH_2(CH_2)_{19}CH_3$), 1.66 (quintet, J = 6.9 Hz, 2H, $OCH_2CH_2(CH_2)_{19}CH_3$), 3.97 (q, J = 6.6 Hz, 2H, $OCH_2CH_2(CH_2)_{19}CH_3$); ^{13}C NMR ($CDCl_3$/MeOH-d_4) δ 14.22, 23.01, 25.87, 29.61, 29.71, 29.93, 29.97, 30.04, 30.73 (d, $J_{C,P}$ = 7.4 Hz), 32.29, 67.27 (d, $J_{C,P}$ = 5.6 Hz); ^{31}P NMR ($CDCl_3$/MeOH-d_4) δ 20.66; MS: $[M - H]^-$ at m/z 405.1.

Molecular Modeling of the LPA_2 Receptor

The inactive and active models of LPA_2 were previously developed in our research group (Sardar et al., 2002). Briefly, the inactive model of LPA_2 was developed by homology modeling using the MOE (molecular operating environment) program (version 2002:01; Chemical Computing Group, Montreal, ON, Canada) and was based on the bovine rhodopsin crystal structure (Palczewski et al., 2000). The active model of the LPA_2 receptor was developed via homology modeling using MOE and was based on the validated model of $S1P_1$ (Parrill et al., 2000). Autodock 3.0 (Morris et al., 1996, 1998) was used to calculate the docked energies for FAP-12 with both the inactive and active model of LPA_2. Automated docking using the Lamarckian genetic algorithm (Morris et al., 1998) was applied to generate 100 complexes of FAP with the LPA_2 receptor (inactive and active forms) and LPA with the LPA_2 receptor (active form), to evaluate the binding region of the ligand. The best complex for each receptor, in terms of energy and binding position of the ligand, was energy minimized with the MMFF94 force field (Halgren, 1996) to a root-mean-square gradient of 0.01 kcal/mol/Å to allow the receptor to adapt to the presence of the ligand. The ligands were then removed from the minimized receptor-ligand complexes and 100 additional complexes were generated with Autodock to re-examine the binding energy after allowing the receptor to acclimatize to the ligand. Autodock 3.0 allows full flexibility of ligand torsion angles but does not provide opportunity for protein side chains to adapt to the presence of a ligand. Thus, the best protein-ligand complex found in an initial docking run was geometry optimized to allow protein side chains to optimize in the presence of the ligand. The ligand was then removed and docked back into the protein to obtain a final docked energy that better reflects the induced fit that occurs when protein-ligand binding occurs. If a conformation similar to the one before minimization was not obtained, the docking run was repeated. When the preminimized conformation was located, the complex with the lowest docked energy was chosen as the best complex.

Cells and Cell Culture

Oocytes were harvested and treated as described earlier (Tigyi et al., 1999). RH7777 cells, stably expressing human LPA_2 receptors, were provided by Dr. Kevin Lynch (University of Virginia, Charlottesville, VA). All cell lines were maintained in Dulbecco's modified Eagle's medium, containing 10% fetal bovine serum and 2 mM glutamine, containing 250 μg/ml G418 for the stable transfectants. RH7777 cells stably expressing LPA_1 and LPA_3 receptors have been generated by our group and characterized elsewhere (Fischer et al., 2001). N1E-115 and IEC-6 cells were purchased from American Type Culture Collection (Manassas, VA).

Cellular Assays

Electrophysiological recording from *X. laevis* oocytes was done using the standard two-electrode voltage clamp technique (Tigyi et al., 1999). Monitoring of intracellular Ca^{2+} changes using Fura-2 acetoxymethyl ester fluorescent indicator (Tigyi et al., 1999) and ligand-induced [^{35}S]GTP-γ-S binding assays (Parrill et al., 2000) was performed as described in our previous publications. FAP samples were prepared fresh from methanolic stock solutions by diluting them in perfusion buffer directly before application. LPA samples were prepared the same way from a bovine serum albumin-complexed stock solution.

Lipid Phosphate Phosphatase Assay

Lipid phosphate phosphatase (LPP) activity was measured as described previously (Yokoyama et al., 2002). Competitive inhibition of FAP-12 on LPP activity was analyzed according to the surface dilution kinetics model (Carman et al., 1995; Dillon et al., 1997). A 100,000*g* pellet from mouse fibroblasts overexpressing mouse LPP1 was used as the enzyme source, and the reaction was performed in the presence of 2 mol% ([lipid]/([lipid] + [Triton X-100]) [^{32}P]LPA (50 μM, 2×10^4 cpm/assay), 2.5 mM Triton X-100, and indicated amount of competitors, including FAP-12. The released [^{32}P]phosphate was extracted and measured.

DNA Fragmentation Assay

The topoisomerase inhibitor camptothecin induces DNA fragmentation and apoptosis in rat IEC-6 intestinal epithelial cells that can be prevented by LPA (Deng et al., 2002). To assess the agonist properties of FAP-12, IEC-6 cells were exposed to 20 μM camptothecin for 6 h with or without FAP-12 (10 μM) or LPA (10 μM) pretreatment (15 min before camptothecin) and DNA fragmentation was measured using an enzyme-linked immunosorbent assay method with the cell death detection enzyme-linked immunosorbent assay kit from Roche (Indianapolis, IN). Briefly, cells were harvested and lysed in DNA lysis buffer for 30 min and centrifuged at 200 rpm for 10 min. An aliquot of the supernatant was incubated with anti-histone-biotin plus anti-DNA peroxidase conjugated antibody in 96-well streptavidin-coated plates on a shaker for 2 h. After washing with the incubation buffer, 100 μl of substrate buffer was added to each well and incubated for an additional 5 to 10 min. DNA absorbance was read at 405 nm in a microplate reader. Duplicates of the samples were used to quantify protein using the bicinchoninic acid assay kit from Pierce (Rockford, IL). DNA fragmentation was expressed as absorbance units per microgram of protein per minute.

RT-PCR Analysis of LPA Receptor Expression

To assess the expression of LPA receptor subtypes in N1E-115 cells, RT-PCR analysis was performed using a primer set and PCR protocol described in previous publications (Tigyi et al., 1999; Fischer et al., 2001).

Data Analysis

The significance of differences between the groups was determined using the Student's *t* test. Values were considered significantly different at $p < 0.05$. The antagonists' binding constant, K_i, was estimated by the method of Cheng (2002), as follows: $K_i = IC_{50}/(1 + ([LPA]/EC_{50})^{nH})$, where IC_{50} is the half-effective concentration of the inhibitor, EC_{50} is the half-effective concentration of the agonist (LPA), n_H is the slope function (Hill- or cooperativity-exponent) in the logistic function that describes the agonist's activation curve, and [LPA] is the concentration of LPA against which the antagonist was being tested.

Results

The synthetic pathway used to generate FAPs is shown in Fig. 1. Molecular structures were verified by NMR and mass spectrometry, and all spectral data were consistent with the assigned structures (see *Materials and Methods*).

FAPs with hydrocarbon chain lengths of 4, 8, 12, 18, and 22 were tested for their ability to enhance or inhibit LPA-induced Cl^- currents in *X. laevis* oocytes. None of the FAP compounds activated Cl^- currents in the oocytes when applied up to 10 μM (data not shown). In contrast, all FAPs

inhibited LPA-induced Cl^- currents with varying potency. Dose-inhibition measurements revealed a strong correlation between chain length and inhibitory action (Fig. 2A). The lowest IC_{50} was observed using FAP-12 and FAP-8 (IC_{50} = 2.4 ± 1 and 6 ± 1 nM, respectively, against 5 nM oleoyl-LPA). FAPs with shorter or longer hydrocarbon chains than 12 were less effective in inhibiting the LPA responses.

When coapplied with LPA, FAP-12 shifted the LPA dose-response curve to the right, suggesting a competitive mechanism for the antagonist activity (Fig. 2B). In *X. laevis* oocytes the LPA dose-response curve has been shown to be biphasic and has been attributed to the presence of both high- and low-affinity binding sites (Guo et al., 1996; Liliom et al., 1996b). When the LPA activation curve was measured in the presence of FAP-12, it could be fitted by a simple Langmuir isotherm, suggestive of only one binding site (Fig. 2B). The activation curves measured in the absence and presence of the inhibitor run parallel at high LPA concentrations. Consequently, FAP-12 seems to inhibit only the high-affinity LPA binding site.

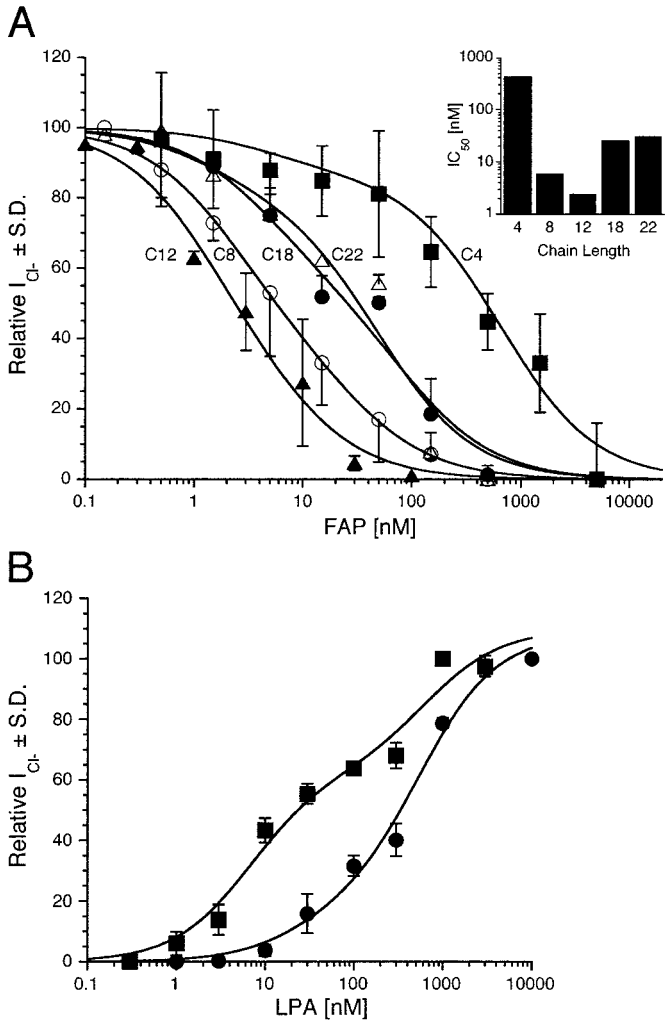

Fig. 2. Pharmacological characterization of the FAPs on LPA-elicited Cl^- currents in *X. laevis* oocytes. A, 5 nM LPA 18:1 mixed with increasing concentrations of FAP-4 (■), -8 (○), -12 (▲), -18 (●), or -22 (△) was superfused over oocytes and peak Cl^- current amplitudes were measured. 100% represents the peak amplitude of the Cl^- current activated by 5 nM LPA, and 0% corresponds to baseline holding current. The bar graph represents the IC_{50} values for each FAP compound. IC_{50} values were 423 ± 150, 6 ± 1, 2.4 ± 1, 26 ± 12, and 32 ± 16 nM for FAP-4, -8, -12, -18, and -22, respectively. Data points represent the average of at least three measurements ± S.D. B, effect of FAP-12 on the LPA dose-response curve in *X. laevis* oocytes. Oocytes were treated with increasing concentrations of LPA (18:1) (■) alone, or mixed with 30 nM FAP-12 (●). 100% represents the peak amplitude for the maximal LPA-activated Cl^- current, and 0% corresponds to baseline holding current. EC_{50} values were 30 ± 8 and 300 ± 40 nM for LPA and LPA + 30 nM FAP-12, respectively. Data points represent the average values of at least three experiments ± S.D.

To characterize the effects of the FAP compounds in a mammalian system, we chose the RH7777 rat hepatoma cell line, which does not respond to LPA or S1P in a variety of cellular assays, including Ca^{2+} mobilization, and does not express any of the known LPA and S1P receptors as monitored by RT-PCR (Zhang et al., 1999). In cells stably expressing LPA_1, FAP-12 weakly inhibited LPA-induced Ca^{2+}-mobilization (Fig. 3). In contrast, FAP-12 alone did not elicit intracellular Ca^{2+} transients when applied up to 10 μM (data not shown). Surprisingly, LPA_2-expressing cells showed a dose-dependent increase in intracellular Ca^{2+} mobilization in response to FAP-10 and FAP-12, with EC_{50} values of 3.7 ± 0.2 μM and 700 ± 22 nM, respectively (Fig. 4A). FAP-14 was found to be a weak agonist, when applied at 10 μM. In contrast, no other FAP analog elicited Ca^{2+} mobilization, or inhibited the LPA response when applied in concentrations up to 10 μM. The maximal response to FAP-12 was 50% of that elicited by LPA, suggesting that FAP-12 was a partial agonist of the LPA_2 receptor. When a concentration of 10 μM was applied only FAP-10, FAP-12 and FAP-14 showed significant agonist activity (Fig. 4B) with FAP-10 being the most efficacious.

Computational docking studies were used to evaluate the

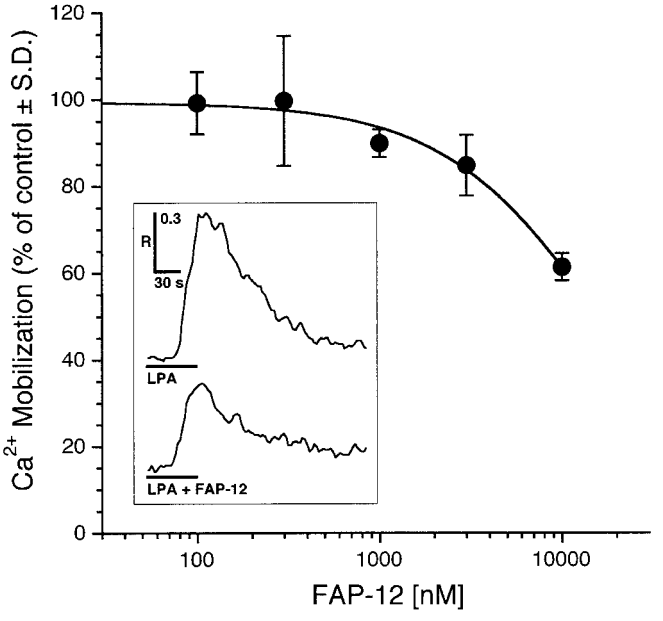

Fig. 3. Inhibition of LPA-induced Ca^{2+} mobilization by FAP-12 in RH7777 cells expressing LPA_1 receptors. Cells were exposed to 250 nM LPA (18:1) mixed with increasing concentrations of FAP-12. Peak areas of Ca^{2+} responses were measured. 100% represents the peak area of the Ca^{2+} transient elicited by 250 nM LPA, and 0% corresponds to baseline fluorescence. Ca^{2+} mobilization was measured as the ratio of fluorescence values at 340 and 380 nm. Data points represent the average from at least three experiments ± S.D. Inset, representative time-courses for Ca^{2+} transients induced by 250 nM LPA alone or by coapplication of 250 nM LPA with 10 μM FAP-12. R is the ratio of fluorescence measured at 340 and 380 nm.

interactions of LPA and FAP with LPA_2. When LPA (18:1) was docked against the active LPA_2 model, the lowest docked free energy was −15.08 kcal/mol. The binding pocket of LPA (18:1) was in the transmembrane domain with the phosphate group of LPA forming ion pairs with arginine 107 and lysine 278 (Fig. 5A) and the 2-hydroxyl group of LPA hydrogen bonding with glutamine 108.

FAP-12 was docked against both the active and inactive models of LPA_2. The lowest docked energy obtained upon evaluation of FAP-12 with the inactive form of LPA_2 was −9.98 kcal/mol. A more favorable docked energy, −12.44 kcal/mol, was obtained when FAP-12 was docked against the active form of LPA_2, consistent with the agonist effect observed experimentally. The binding pocket of FAP-12 was located in the transmembrane domain and ion pairs were observed between the phosphate and two cationic residues, arginine 107 and lysine 278 of LPA_2 (Fig. 5B). These interactions are consistent with our previous studies on the binding of LPA to the LPA receptors (Wang et al., 2001; Sardar et al., 2002).

Docking studies between FAP-8, FAP-10 (Fig. 5C), FAP-14, and FAP-18 were performed using the active LPA_2 model, with resulting docked energies of −9.17, −10.46, −12.06, and −10.84 kcal/mol, respectively. The binding mode observed for these structures was similar to that observed for FAP-12. All four of these compounds had lower (less favorable) docked energies than FAP-12, as expected based on the experimental observation that FAP-12 had the lowest EC_{50}. However, the relative energies did not correlate further with the experimentally observed receptor activation. Several factors probably contribute to this discrepancy. First, energies from docking studies are most reflective of binding affinity rather than

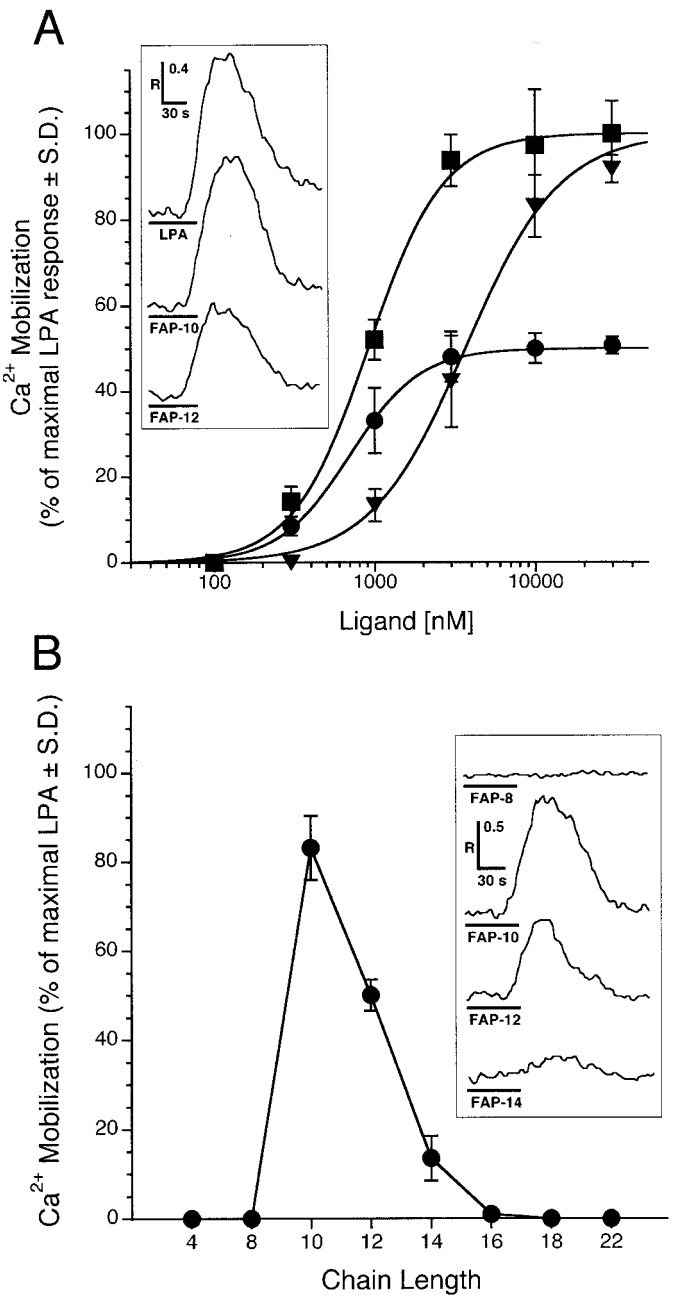

Fig. 4. A, dose-dependent activation of LPA_2 by FAPs. Increasing concentrations of LPA (■), FAP-10 (▼), or FAP-12 (●) were applied, and the peak areas of Ca^{2+} responses were measured in RH7777 cells stably expressing LPA_2. The EC_{50} values for FAP-10 and FAP-12 were 700 ± 22 nM and 3.7 ± 0.2 μM, respectively. 100% represents the peak area for maximal LPA-activated Ca^{2+} mobilization, and 0% corresponds to baseline. Data points represent the average of at least three measurements ± S.D. Inset, comparison of time courses of maximal Ca^{2+} responses to LPA (18:1), FAP-10, and FAP-12 in LPA_2-expressing RH7777 cells. LPA, FAP-10, or FAP-12 (30 μM) was applied. R is the ratio of fluorescence measured at 340 and 380 nm. B, chain length dependence of FAP agonist activity in RH7777 cells expressing LPA_2. FAP compounds were applied at 10 μM, and peak areas of Ca^{2+} responses were measured. Data points represent the average of at least three measurements ± S.D. Inset, comparison of time courses of Ca^{2+} transients elicited by 10 μM FAP-8, -10, -12, and -14. R is the ratio of fluorescence measured at 340 and 380 nm.

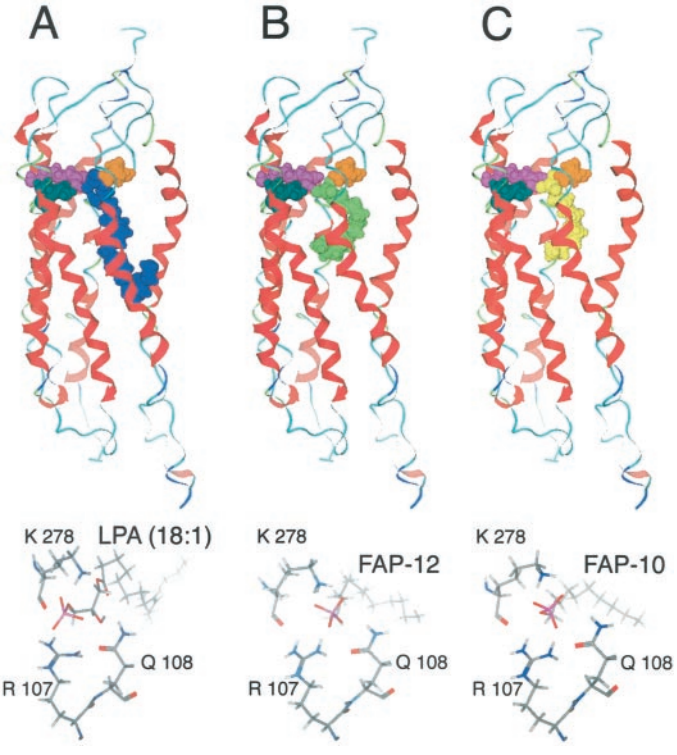

Fig. 5. Model of the LPA_2 receptor docked with LPA (18:1) (A), FAP-12 (B), and FAP-10 (C). LPA_2 is shown as a ribbon model (side view, top) with the ligands LPA (18:1) (blue), FAP-12 (green), and FAP-10 (yellow) as space-filling models. Residues R 107 (magenta), Q 108 (teal), and K 278 (orange) are also shown as space-filling models. Close-up view (top view, bottom) of critical interactions between LPA_2 residues and the phosphate group of the three ligands is shown.

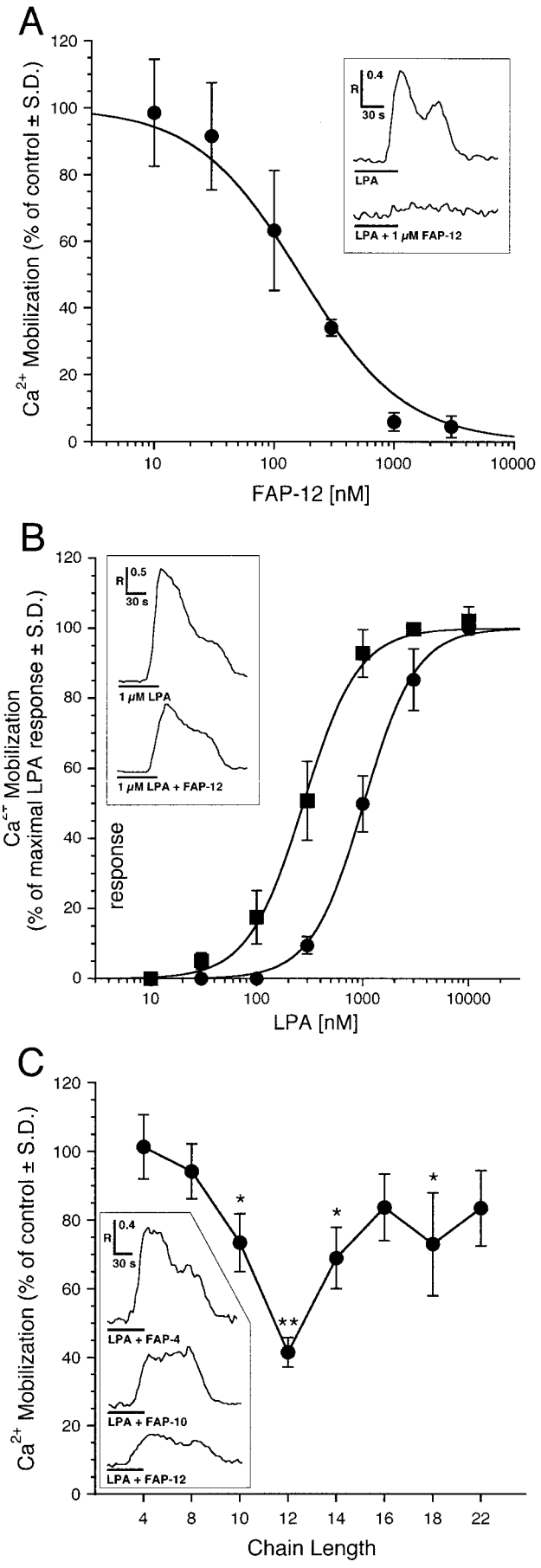

receptor activation. Second, binding is governed by the free energy change that occurs when a ligand moves from one environment (often aqueous solution) to another (a protein binding site). The docked energies represent only the enthalpic part of the free energy. The entropic part of the free energy, which consists of changes in conformational freedom and solvation effects, may be an important contributor to the differences in FAP compound activity.

RH7777 cells stably expressing the LPA_3 receptor did not respond to any of the FAPs by Ca^{2+} mobilization when applied up to 10 μM (data not shown). However, FAP-12 dose dependently inhibited LPA-induced Ca^{2+} mobilization with a K_i of 90 nM (Fig. 6A). Coapplication of 300 nM FAP-12 with LPA shifted the dose-response curve of LPA to the right, increasing the EC_{50} value from 300 ± 14 to 1000 ± 30 nM and suggesting a competitive type of inhibition (Fig. 6B).

All FAPs were tested for their ability to inhibit LPA-elicited Ca^{2+}-mobilization in cells expressing LPA_3. Applied at a concentration of 200 nM, FAP-12 was the most effective (60% inhibition), followed by FAP-10, -14, and -18 (~25% inhibition) (Fig. 6C). FAP-4, -8, -16, and -22 did not inhibit the LPA response significantly at this concentration.

To determine whether the effects of FAPs were selective to LPA receptors, we examined the most potent analog, FAP-12, on responses elicited by various mammalian G-protein coupled receptors. In oocytes expressing poly(A)$^+$ mRNA from rat brain, responses elicited by serotonin (10 μM), kainate (100 μM), and glutamate (10 μM), which are mediated through the inositol trisphosphate-Ca^{2+} pathway, were tested for interference by FAPs. In the presence of 10 μM FAP-12, these responses relative to control were 103 ± 8, 95 ± 12, and 106 ± 7% (n = 3), respectively. The lack of inhibition indicates that FAP-12 did not inhibit these neurotransmitter receptors or the second-messenger systems mediating Ca^{2+}-activated Cl^- currents. Additionally, in RH7777 cells, FAP-12 (10 μM) did not affect ATP-induced (1 μM) Ca^{2+} mobilization (101 ± 10% of ATP alone control, n = 3) indicating that in this mammalian cell line, just as in *X. laevis* oocytes, the compound did not interfere with ligand-induced Ca^{2+} transients.

The effects of FAP-12 were also tested on S1P receptors. GTP-γ-S loading assays were performed on RH7777 cells stably expressing $S1P_1$. FAP-12, when coapplied with S1P (300 nM) up to 10 μM, neither enhanced nor inhibited the

Fig. 6. A, FAP-12 inhibits LPA (18:1)-induced Ca^{2+} mobilization in RH7777 cells stably expressing LPA_3 in a dose-dependent manner. LPA (250 nM; 18:1) was mixed with increasing concentrations of FAP-12. The K_i value was 90 nM. Data points represent the average of at least three measurements ± S.D. Inset, time courses of Ca^{2+} mobilization after application of 250 nM LPA alone or together with 1 μM FAP-12. R is the ratio of fluorescence measured at 340 and 380 nm. B, FAP-12 shifts the LPA dose-response curve to the right. Cells were exposed to increasing concentrations of LPA (■) or mixed with 300 nM FAP-12 (●). EC_{50} values were 300 ± 14 nM for LPA and 1000 ± 30 nM for LPA + 300 nM FAP-12. Data points represent the average of peak areas from at least three measurements ± S.D. Inset, time courses of Ca^{2+} mobilization after application of 1 μM LPA alone or together with 300 nM FAP-12. R is the ratio of fluorescence measured at 340 and 380 nm. C, the relationship between FAP chain length and inhibition of LPA-elicited Ca^{2+} mobilization through LPA_3 in RH7777 cells. Each FAP compound (200 nM) was mixed with 250 nM LPA (18:1), and the elicited Ca^{2+} peak areas were measured. Data points represent the average of at least three measurements ± S.D. Inset, time courses of Ca^{2+} mobilization after coapplication of 250 nM LPA with 200 nM FAP-4, -10, and -12. R is the ratio of fluorescence measured at 340 and 380 nm.

TABLE 1
Effect of FAP-12 on S1P receptors

	FAP-12 Alone		S1P + FAP-12		
	FAP-12	Response	S1P	FAP-12	Response
	μM	*% of vehicle*	*μM*	*μM*	*% of S1P*
$S1P_1$	10	95 ± 5[a]	0.3	10	97 ± 4[a]
$S1P_2$	10	100 ± 0[b]	0.3	1	99 ± 11[b]
$S1P_3$	10	100 ± 0[b]	1	1	104 ± 13[b]
$S1P_5$	10	90 ± 5[a]	0.3	10	101 ± 2[a]

[a] Results were obtained using [^{35}S]GTP-γ -S binding assay.
[b] Results were obtained using intracellular Ca^{2+}-monitoring.

substantial S1P-induced GTP loading. FAP-12 alone did not induce GTP loading in these cells (data not shown). Similar results were obtained with RH7777 cells transiently transfected with S1P5 (Table 1). S1P elicits dose-dependent Ca^{2+} transients in RH7777 cells expressing $S1P_2$ or $S1P_3$. FAP-12 did not induce Ca^{2+} mobilization in RH7777 cells transiently transfected with $S1P_2$ or $S1P_3$, when applied in concentrations as high as 10 μM, nor did it affect S1P-elicited Ca^{2+} transients (Table 1). We could not test FAP-12 on $S1P_4$ receptors, because, in our hands, this receptor did not respond to S1P in the GTP-γ-S loading or Ca^{2+}-mobilization assays.

To test whether FAP-12 interacts with LPP, a key enzyme of LPA degradation, enzymatic activity was measured in the absence or presence of FAP-12. LPP activity decreased to 73, 58, and 39% of control, when FAP-12 was added in 2-, 4-, and 8-fold excess, respectively (data not shown). This result suggests that FAP12 also interferes with the LPP-mediated degradative pathway of LPA.

To confirm the agonist properties of FAP-12 and FAP-10 on LPA_2, these compounds were tested in N1E-115 neuroblastoma cells for Ca2+ mobilization effect (Fig. 7A). N1E-115 cells express only LPA_2 receptor transcripts (Fig. 7B) and respond to LPA with a transient elevation in $[Ca^{2+}]_i$. FAP-12 and FAP-10 both elicited Ca^{2+} transients in these neuroblastoma cells, confirming their agonist properties in a cell line that endogenously expresses only the LPA_2 receptor subtype. To further characterize the agonist properties of FAP-12 (Fig. 7C), we examined its effect in an apoptosis protection assay using IEC-6 cells. These cells express predominantly LPA_2 along with lesser amounts of LPA_1 (Deng et al., 2002). In these cells, FAP-12 applied at 10 μM elicited a significant decrease in camptothecin-induced DNA fragmentation that was comparable with the effect of LPA (10 μM). The results obtained from N1E-115 and IEC-6 cells lend strong support to the LPA-like agonist properties of FAPs in cell lines that express the LPA_2 receptor subtype.

Discussion

The phospholipid growth factors LPA and S1P are involved in numerous physiological and pathological processes, including regulation of cell proliferation and differentiation, apoptosis, Ca^{2+}-homeostasis (Goetzl et al., 2000; Tigyi, 2001) and tumor cell invasion (Umezu-Goto et al., 2002), and atherosclerosis (Siess et al., 1999). Given that most cells express multiple PLGF receptor subtypes, the lack of subtype-specific agonists and antagonists for LPA receptors remains a limiting factor for the PLGF field. In an effort toward the rational design of such ligands, structural models of the PLGF receptors have been developed recently (Parrill et al., 2000; Wang et al., 2001; Sardar et al., 2002). Based on computational modeling of the ligand-receptor interactions, we deduced and partially validated a model for receptor activation. The model assigned distinct functions to the polar headgroup and the hydrophobic tail within the LPA pharmacophore. In this model, the phosphate headgroup interacts with two positively charged conserved residues in the third and seventh transmembrane helices (Wang et al., 2001), whereas the hydrocarbon tail interacts with hydrophobic side-chains of amino acid residues lining the interhelical pocket (Sardar et al., 2002). These hydrophobic interactions are predicted to be necessary for activation of the receptor (Fischer et al., 2001; Wang et al., 2001). Specific recognition of S1P versus LPA is achieved through hydrogen bonding between the hydroxyl group of LPA and a glutamine or by ion pairing between the amino group of S1P and a glutamate in the third transmembrane helix conserved in the corresponding receptor subfamilies (Wang et al., 2001). The two-point pharmacophore is consistent with the experimentally established structure-activity relationships of LPA (Lynch and Macdonald, 2002; Sardar et al., 2002).

Our group (Fischer et al., 2001) and Dr. Lynch's group (Heise et al., 2001) have reported on LPA antagonists that show receptor subtype selectivity. A systematic screening of 2-OH-substituted *N*-acyl ethanolamide phosphates led to the discovery of a benzyl-4-oxybenzyl derivative of ethanolamine phosphate, of which the *S*-enantiomer exhibited selective antagonism of LPA_1 over LPA_3, whereas it did not affect the LPA_2 receptor (Heise et al., 2001). We found that dioctyl phosphatidic acid and dioctylglycerol pyrophosphate were weak antagonists of LPA_1 and strong antagonists for LPA_3, whereas long-chain analogs (18:1) were not inhibitors of LPA receptors (Fischer et al., 2001). It is important to note that short-chain LPA (8:0) was neither an agonist nor an antagonist in this system (Fischer et al., 2001). Both dioctylglycerol pyrophosphate and (*S*)-2-benzyl-4-oxybenzyl-*N*-acyl ethanolamide phosphate have a negatively charged phosphate head group. They also have two hydrocarbon side chains, unlike the physiological ligand, LPA. Therefore, both the length and size of the hydrophobic tail seems to affect the ability to activate or inhibit LPA receptors. Based on the two-point pharmacophore, we hypothesized that modifications within the hydrophobic tail of the ligand might have profound effects in determining agonist or antagonist behavior and therefore might allow identification of molecules with selective antagonistic properties.

Our earlier work (Bittman et al., 1996; Liliom et al., 1996), as well as of that of others (Hooks et al., 1998; Heise et al., 2001), has shown that the glycerol backbone can be replaced by serine, tyrosine, or ethanolamine but maintain the LPA

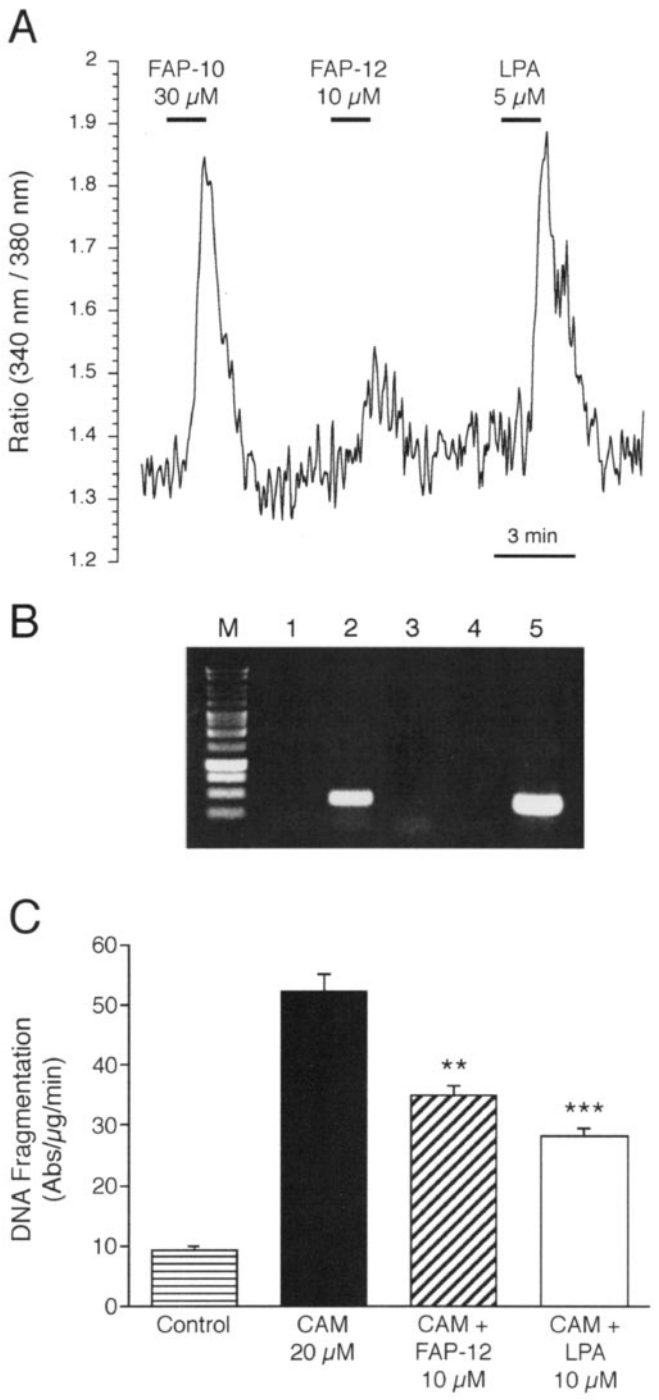

Fig. 7. Agonist properties of FAPs in cells that endogenously express LPA_2. A, time course of a representative experiment monitoring intracellular Ca^{2+} concentration in N1E-115 cells. FAP-10 (30 μM), -12 (10 μM), and LPA 18:1 (5 μM) were applied consecutively to N1E-115 cells and the resulting changes in $[Ca^{2+}]_i$ were recorded. B, RT-PCR study of LPA receptor transcripts in N1E-115 cells. M, molecular weight marker; 1, LPA_1; 2, LPA_2; 3, LPA_3; 4, negative control (no template); 5, beta actin. C, FAP-12 mimics the antiapoptotic effect of LPA in IEC-6 cells. Camptothecin (20 μM) induces apoptosis accompanied by DNA fragmentation within 6 h. LPA (10 μM) or FAP-12 (10 μM) both significantly reduced camptothecin-induced DNA fragmentation (mean $\pm$ S.E.M., $n = 3$).

mimetic effect of these lipid phosphate analogs. Fatty alcohol phosphates provide the simplest set of easy to synthesize analogs required to delineate the minimal structural requirement for a ligand using this hypothesis. For this reason we synthesized a series of FAP molecules with carbon chain lengths from 4 to 22 and characterized their effects on individual LPA and S1P receptor subtypes.

Pharmacological analysis of the FAP series supports our hypothesis that the ionic headgroup attached to a hydrophobic tail are sufficient to make them ligands for all three LPA receptors, although with markedly different efficacies, potencies, and selectivities. FAP-10 and FAP-12 were specific agonists for LPA_2 with EC_{50} values of 3.7 $\pm$ 0.2 μM and 700 $\pm$ 22 nM, respectively, and specific antagonists for LPA_3. FAP-12 also weakly inhibited LPA_1. The decyl and dodecyl chain seem to be unique, which suggests that LPA_2 differs from the other two receptors in that it is activated by these relatively short-chain analogs. FAP molecules with carbon chain lengths shorter than 10 or longer than 14 did not affect LPA_2 and were weaker inhibitors of LPA_3 than FAP-12. Thus, the present results emphasize that acyl chain length plays a significant role in the ligand properties of LPA-like pharmacophores and establishes a distinguishing role in ligand recognition between the different LPA receptor subtypes. Furthermore, FAPs lack the glycerol backbone; thus, the present findings provide compelling evidence that it is not required for ligand activity. These observations are in complete agreement with earlier structure-activity studies in which LPA receptors showed a high degree of tolerance to analogs with serine, tyrosine, or ethanolamine in place of the glycerol backbone (Sugiura et al., 1994; Jalink et al., 1995; Lynch et al., 1997; Hooks et al., 1998).

X. laevis oocytes express three pharmacologically distinguishable receptors for LPA (Liliom et al., 1996b; Fischer et al., 1998). This heterogeneity is reflected in the dose-response curve, which is best described by assuming multiple sites with different high and low affinity for LPA (Guo et al., 1996; Liliom et al., 1996b). Our experiments indicate that FAPs block only the high-affinity site (Fig. 2B). Thus far, two high-affinity LPA sites have been identified in oocytes: the PSP24 (Guo et al., 1996) and LPA_1 receptors (Kimura et al., 2001). Which of these is inhibited by FAPs remains unclear. The human ortholog of the LPA_1 receptor was only weakly inhibited by FAP-12 in concentrations in the high micromolar range (Fig. 3). The highly conserved nature of mammalian and *X. laevis* LPA_1 tends to argue against the hypothesis that the inhibitor would target LPA1. On the other hand, overexpression of *X. laevis* LPA_1 in *X. laevis* oocytes augmented the endogenous LPA response (Kimura et al., 2001), whereas the human ortholog did not (Yokoyama et al., 2002). Interestingly, the chain length-dependence of the inhibitory potencies of FAPs in *X. laevis* oocytes (Fig. 2A) and in LPA_3-expressing RH7777 cells (Fig. 6C) is very similar despite the consensus that oocytes do not express an LPA_3 receptor subtype (Kimura et al., 2001).

FAPs did not activate or inhibit S1P receptors, suggesting that this cluster within the EDG receptor family is fundamentally different from the LPA receptor cluster despite several similarities in ligand recognition. Based on earlier structure-activity measurements, a free amino group on the sphingoid backbone seems to be necessary for ligand recognition of the S1P receptors (Van Brocklyn et al., 1998). This group is necessary for ligand binding (Parrill et al., 2000) and provides selectivity for these receptors to distinguish S1P from LPA (Wang et al., 2001). The absence of this free amino group in the FAP structure might explain the lack of effect of

these molecules on S1P receptors. The agonist and antagonist effects of FAP-12 seem to be specific for LPA receptors because it did not modify the function of other heterologously expressed GPCRs in the *X. laevis* bioassay or RH7777 cells. The agonist properties of FAP-12 were confirmed in N1E-115 and IEC-6 cells that endogenously express LPA_2 receptor subtype (Fig. 7). Thus, the present data identify FAP-12 as the first LPA_2-selective agonist. Computational docking studies of FAP-8, -10, -12, -14, -18, and LPA against the active form of LPA_2 suggest that the greatest affinity for all structures occurs in an overlapping region in the receptor. The energies observed for FAP-12 binding to the active and inactive models of the LPA_2 receptor, −12.44 kcal/mol versus −9.98 kcal/mol, are consistent with the experimental observation that FAP-12 is a partial agonist and thus interacts more strongly with the active conformation of the LPA_2 receptor. The lowest docked energy was observed for FAP-12 binding to the active model, a finding consistent with the observed lowest EC_{50} value (700 ± 22 nM) for this structure. Thus, the present results provide new refinements to our computational models.

FAP-12 inhibits LPA degradation by LPP, indicating that the simplified structure of the FAP molecule is also recognized by a key enzyme in the established degradation pathway of LPA. This observation suggests that FAP-12 will have at least three molecular targets: the LPA_3 and LPA_2 receptors and LPP enzymes.

The two-point pharmacophore for LPA receptor activation, which is based on our atomic resolution structural models of the PLGF receptors, makes the rational design of receptor subtype-selective agonists and antagonists possible, opening an important new avenue of research in the PLGF field. This approach identified FAPs as selective inhibitors of LPA_3 and the first subtype-specific agonists of LPA_2 receptors. Although the compounds identified here are not themselves likely to be useful clinically, they could serve as lead compounds for further development. Moreover, the differential effects of the acyl chain length derivatives of FAPs point to an important concept in designing subtype-selective reagents.

References

An S, Bleu T, Zheng Y, and Goetzl EJ (1998) Recombinant human G protein-coupled lysophosphatidic acid receptors mediate intracellular calcium mobilization. *Mol Pharmacol* **54:**881–888.

Bandoh K, Aoki J, Taira A, Tsujimoto M, Arai H, and Inoue K (2000) Lysophosphatidic acid (LPA) receptors of the EDG family are differentially activated by LPA species. Structure-activity relationship of cloned LPA receptors. *FEBS Lett* **478:** 159–165.

Bittman R, Swords B, Liliom K, and Tigyi G (1996) Inhibitors of lipid phosphatidate receptors: N-palmitoyl-serine and N-palmitoyl-tyrosine phosphoric acids. *J Lipid Res* 37:391–398.

Carman GM, Deems RA, and Dennis EA (1995) Lipid signaling enzymes and surface dilution kinetics. *J Biol Chem* **270:**18711–18714.

Chan CK and Durieux ME (1997) Differential inhibition of lysophosphatidate signaling by volatile anesthetics. *Anesthesiology* **86:**660–669.

Cheng HC (2002) The power issue: determination of KB or Ki from IC50. A closer look at the Cheng-Prusoff equation, the Schield plot and related power equations. *J Pharmacol Toxicol Methods* **46:**61–71.

Chun J, Goetzl EJ, Hla T, Igarashi Y, Lynch KR, Moolenaar W, Pyne S, and Tigyi G (2002) International Union of Pharmacology. XXXIV. Lysophospholipid receptor nomenclature. *Pharmacol Rev* **54:**265–269.

Contos JJ, Ishii I, and Chun J (2000) Lysophosphatidic acid receptors. *Mol Pharmacol* **58:**1188–1196.

Deng W, Balazs L, Wang D-A, Van Middlesworth L, Tigyi G, and Johnson LR (2002) Lysophosphatidic acid protects and rescues intestinal epithelial cells from radiation- and chemotherapy-induced apoptosis. *Gastroenterology* **123:**206–216.

Dillon DA, Chen X, Zeimetz GM, Wu WI, Waggoner DW, Dewald J, Brindley DN, and Carman GM (1997) Mammalian Mg^{2+}-independent phosphatidate phosphatase (PAP2) displays diacylglycerol pyrophosphate phosphatase activity. *J Biol Chem* **272:**10361–10366.

Fischer DJ, Liliom K, Guo Z, Nusser N, Virag T, Murakami-Murofushi K, Kobayashi S, Erickson JR, Sun G, Miller DD, et al. (1998) Naturally occurring analogs of lysophosphatidic acid elicit different cellular responses through selective activation of multiple receptor subtypes. *Mol Pharmacol* **54:**979–988.

Fischer DJ, Nusser N, Virag T, Yokoyama K, Wang D, Baker DL, Bautista D, Parrill AL, and Tigyi G (2001) Short-chain phosphatidates are subtype-selective antagonists of lysophosphatidic acid receptors. *Mol Pharmacol* **60:**776–784.

Goetzl EJ, Lee H, Dolezalova H, Kalli KR, Conover CA, Hu YL, Azuma T, Stossel TP, Karliner JS, and Jaffe RB (2000) Mechanisms of lysolipid phosphate effects on cellular survival and proliferation. *Ann NY Acad Sci* **905:**177–187.

Gueguen G, Gaige B, Grevy JM, Rogalle P, Bellan J, Wilson M, Klaebe A, Pont F, Simon MF, and Chap H (1999) Structure-activity analysis of the effects of lysophosphatidic acid on platelet aggregation. *Biochemistry* **38:**8440–8450.

Guo Z, Liliom K, Fischer DJ, Bathurst IC, Tomei LD, Kiefer MC, and Tigyi G (1996) Molecular cloning of a high-affinity receptor for the growth factor-like lipid mediator lysophosphatidic acid from Xenopus oocytes. *Proc Natl Acad Sci USA* **93:** 14367–14372.

Halgren TA (1996) Merck molecular force field. I. Basis form scope parameterization and performance of MMFF94*. *J Comput Chem* **17:**490–519.

Heise CE, Santos WL, Schreihofer AM, Heasley BH, Mukhin YV, Macdonald TL, and Lynch KR (2001) Activity of 2-substituted lysophosphatidic acid (LPA) analogs at LPA receptors: discovery of a LPA1/LPA3 receptor antagonist. *Mol Pharmacol* **60:**1173–1180.

Hooks SB, Ragan SP, Hopper DW, Honemann CW, Durieux ME, Macdonald TL, and Lynch KR (1998) Characterization of a receptor subtype-selective lysophosphatidic acid mimetic. *Mol Pharmacol* **53:**188–194.

Jalink K, Hengeveld T, Mulder S, Postma FR, Simon MF, Chap H, van der Marel GA, van Boom JH, van Blitterswijk WJ, and Moolenaar WH (1995) Lysophosphatidic acid-induced Ca^{2+} mobilization in human A431 cells: Structure-activity analysis. *Biochem J* **307:**609–616.

Kimura Y, Schmitt A, Fukushima N, Ishii I, Kimura H, Nebreda AR, and Chun J (2001) Two novel Xenopus homologs of mammalian LP_{A1}/EDG-2 function as lysophosphatidic acid receptors in Xenopus oocytes and mammalian cells. *J Biol Chem* **276:**15208–15215.

Liliom K, Bittman R, Swords B, and Tigyi G (1996a) *N*-Palmitoyl-serine and *N*-palmitoyl-tyrosine phosphoric acids are selective competitive antagonists of the lysophosphatidic acid receptors. *Mol Pharmacol* **50:**616–623.

Liliom K, Murakami-Murofushi K, Kobayashi S, Murofushi H, and Tigyi G (1996b) Xenopus oocytes express multiple receptors for LPA-like lipid mediators. *Am J Physiol* **270:**C772–C777.

Lynch KR, Hopper DW, Carlisle SJ, Catalano JG, Zhang M, and MacDonald TL (1997) Structure/activity relationships in lysophosphatidic acid: the 2-hydroxyl moiety. *Mol Pharmacol* **52:**75–81.

Lynch KR and Macdonald TL (2002) Structure-activity relationships of lysophosphatidic acid analogs. *Biochim Biophys Acta* **1582:**289–294.

Morris GM, Goodsell DS, Halliday RS, Huey R, Hart WE, Belew RK, and Olson AJ (1998) Automated docking using a Lamarckian genetic algorithm and an empirical binding free energy function. *J Comput Chem* **19:**1639–1662.

Morris GM, Goodsell DS, Huey R, and Olson AJ (1996) Distributed automated docking of flexible ligands to proteins: Parallel applications of AutoDock 2.4. *J Comput-Aided Mol Des* **10:**293–304.

Palczewski K, Kumasaka T, Hori T, Behnke CA, Motoshima H, Fox BA, Le Trong I, Teller DC, Okada T, Stenkamp RE, et al. (2000) Crystal structure of rhodopsin: a G protein-coupled receptor. *Science (Wash DC)* **289:**739–745.

Parrill AL, Wang D, Bautista DL, Van Brocklyn JR, Lorincz Z, Fischer DJ, Baker DL, Liliom K, Spiegel S, and Tigyi G (2000) Identification of Edg1 receptor residues that recognize sphingosine 1-phosphate. *J Biol Chem* **275:**39379–39384.

Sardar VM, Bautista DL, Fischer DJ, Yokoyama K, Nusser N, Virag T, Wang DA, Baker DL, Tigyi G, and Parrill AL (2002) Molecular basis for lysophosphatidic acid receptor antagonist selectivity. *Biochim Biophys Acta* **1582:**309–317.

Siess W, Zangl KJ, Essler M, Bauer M, Brandl R, Corrinth C, Bittman R, Tigyi G and Aepfelbacher M (1999) Lysophosphatidic acid mediates the rapid activation of platelets and endothelial cells by mildly oxidized low density lipoprotein and accumulates in human atherosclerotic lesions. *Proc Natl Acad Sci USA* **96:**6931–6936.

Sugiura T, Tokumura A, Gregory L, Nouchi T, Weintraub ST, and Hanahan DJ (1994) Biochemical characterization of the interaction of lipid phosphoric acids with human platelets: comparison with platelet activating factor. *Arch Biochem Biophys* **311:**358–368.

Tigyi G (2001) Physiological responses to lysophosphatidic acid and related glycerophospholipids. *Prostaglandins Other Lipid Mediat* **64:**47–62.

Tigyi G, Liliom K, Fischer DJ, and Guo Z (1999) Phospholipid growth factors: identification and mechanism of action, in *Lipid second messengers* (Laychock SG and Rubin RP eds) pp 51–81, CRC Press, Boca Raton, FL.

Tigyi J, Tigyi G, Liliom K, and Miledi R (1997) Local anesthetics inhibit receptors coupled to phosphoinositide signaling in Xenopus oocytes. *Pflueg Arch Eur J Physiol* **433:**478–487.

Umezu-Goto M, Kishi Y, Taira A, Hama K, Dohmae N, Takio K, Yamori T, Mills GB, Inoue K, Aoki J, et al. (2002) Autotaxin has lysophospholipase D activity leading to tumor cell growth and motility by lysophosphatidic acid production. *J Cell Biol* **15:**227–233.

Van Brocklyn JR, Lee MJ, Menzeleev R, Olivera A, Edsall L, Cuvillier O, Thomas DM, Coopman PJ, Thangada S, Liu CH, et al. (1998) Dual actions of sphingosine-1-phosphate: Extracellular through the Gi-coupled receptor Edg-1 and intracellular to regulate proliferation and survival. *J Cell Biol* **142:**229–240.

Wang DA, Lorincz Z, Bautista DL, Liliom K, Tigyi G, and Parrill AL (2001) A single amino acid determines lysophospholipid specificity of the S1P1 (EDG1) and LPA1 (EDG2) phospholipid growth factor receptors. *J Biol Chem* **276:**49213–49220.
Yokoyama K, Baker DL, Virag T, Liliom K, Byun HS, Tigyi G, and Bittman R (2002) Stereochemical properties of lysophosphatidic acid receptor activation and metabolism. *Biochim Biophys Acta* **1582:**295–308.
Zhang G, Contos JJ, Weiner JA, Fukushima N, and Chun J (1999) Comparative analysis of three murine G-protein coupled receptors activated by sphingosine-1-phosphate. *Gene* **227:**89–99.

Address correspondence to: Gabor Tigyi, M.D., Ph.D., Department of Physiology, The University of Tennessee Health Science Center, 894 Union Avenue, Memphis, TN 38163. E-mail: gtigyi@physio1.utmem.edu